

Glauber modeling of high-energy nuclear collisions at sub-nucleon level

C. Loizides¹

¹Lawrence Berkeley National Laboratory, Berkeley, California, USA

Glauber models based on nucleon–nucleon interactions are commonly used to characterize the initial state in high-energy nuclear collisions, and the dependence of its properties on impact parameter or number of participating nucleons. In this article, an extension to the Glauber model is presented, which accounts for an arbitrary number of effective sub-nucleon degrees of freedom, or partonic constituents, in the nucleons. Properties of the initial state, such as the number of constituent participants and collisions, as well as eccentricity and triangularity, are calculated and systematically compared for different assumptions how to distribute the sub-nuclear degrees of freedom and for various collision systems. It is demonstrated that at high collision energy the number of produced particles scales with an average number of sub-nucleon degrees of freedom of between 3 and 5. The source codes for the constituent Monte Carlo Glauber extension, as well as for the calculation of the overlap area and participant density in a standard Glauber model, are made publicly available.

I. INTRODUCTION

Properties of the initial state in high-energy nuclear collisions are commonly calculated using a Glauber model [1]. In these calculations, nuclei are composed out of a set of nucleons, and the nuclear reaction is approximated by successive independent nucleon–nucleon (NN) interactions assuming the nucleons travel in a straight line along the beam axis (eikonal approximation). The so called “optical” Glauber calculations [2, 3] assume a smooth matter density distribution for the makeup of the nuclei, while the Monte Carlo (MC) based models [4, 5] distribute individual nucleons event-by-event, and collision properties are obtained by averaging over multiple events. In both cases, one usually uses a Fermi distribution for the radial direction and a uniform distribution for the solid angle.

These calculations can easily be extended to sub-nucleon level by taking into account three valence quarks per nucleon in the collision process. It has recently been shown [6–10] that particle production at mid-rapidity in high-energy nucleus–nucleus collisions scales almost linearly with the number of quark participants, without the need to introduce a contribution from a hard-scattering component scaling with the number of binary nucleon–nucleon collisions. Further interest in such calculations arises since understanding the observed azimuthal momentum anisotropy as a result of anisotropic pressure gradients formed early-on due to the spatial anisotropy of the initial state in pA and even pp collisions (see Ref. [11] for a recent summary) needs calculations of the initial state in small systems at sub-nucleon level [12].

In this article, an extension of the MC Glauber model is presented, which generalizes the collision process by accounting for an arbitrary, but fixed, number of effective sub-nucleon degrees of freedom, or partonic constituents, in the nucleons. This description is obviously only a crude approximation of the partonic structure of a nucleon, which depends on the momentum transfer (Q^2) and fraction of nucleon momentum (Bjorken- x). However, the constituent MC Glauber calculation can be

used to effectively model the average number of active degrees of freedom, which contribute to soft particle production, and to study the dependence on collision energy and species. In Sec. II the standard MC Glauber model is briefly recalled, while in Sec. III its extension to sub-nucleon level is discussed. Section. IV discusses properties of the initial state, such as the number of constituent participants and collisions, as well as eccentricity and triangularity, calculated for a variety of different assumptions to distribute the sub-nuclear degrees of freedom and for various collision systems. Section. V provides a short summary. The code for the constituent MC Glauber program is described in App. A. Additional calculations of the overlap area and participant density are discussed in App. B.

II. MC GLAUBER CALCULATION

The Glauber calculation of a nucleus–nucleus collision is done as described in Ref. [13]. First, the positions of each of the A nucleons in a nucleus are determined according to the measured charge density distribution of the nucleus extracted from low-energy electron scattering experiments [14]. For spherical nuclei, such as Pb, the distribution is taken to be uniform in azimuthal and polar angles, and a two-parameter Fermi function

$$\rho(r) = \rho_0 \left(1 + \exp \left(\frac{r - R}{a} \right) \right)^{-1} \quad (1)$$

in the radial direction. In Eq. 1, R is the nuclear radius, and a is the skin depth, and the overall normalization ρ_0 is not relevant for the calculation. To mimic a hard-core repulsion potential in the context of the MC Glauber model, one usually requires a minimum internucleon separation (d_{\min}) of 0.4 fm between the centers of the nucleons. These excluded-volume effects of the nucleons distort the resulting nuclear density and can be absorbed by rescaling the charge-density parameters [15]. The standard and rescaled values for Au and Pb nuclei are given in Tab. I, for other nuclei see Ref. [16].

Nucleus	R [fm]	R_s [fm]	a [fm]	a_s [fm]
^{197}Au	6.38 ± 0.13	6.42	0.535 ± 0.053	0.44
^{208}Pb	6.62 ± 0.06	6.65	0.546 ± 0.010	0.46

TABLE I: Standard and rescaled charge-density parameters.

$\sqrt{s_{\text{NN}}}$ [TeV]	0.019	0.2	2.76	5.02	7	13
σ_{NN} [mb]	33	42	64	70	74	78

TABLE II: Values used for σ_{NN} at various $\sqrt{s_{\text{NN}}}$.

Second, the collision impact parameter (b) is determined from $dN/db \propto b$, and the centers of the nuclei are shifted to $(-b/2, 0, 0)$ and $(b/2, 0, 0)$ ¹. Following the eikonal ansatz, the nucleons are assumed to move along a straight trajectory along the beam axis. Their transverse positions are held constant during the short passage time of the two high-energy nuclei, while their longitudinal coordinate does not play a role in the calculation. The nuclear reaction is modeled by successive independent interactions between two nucleons from different nuclei. The interaction strength between two nucleons is parameterized by the nucleon–nucleon inelastic cross section (σ_{NN}). Two nucleons from different nuclei are supposed to collide if their relative transverse distance is less than

$$D = \sqrt{\sigma_{\text{NN}}/\pi}. \quad (2)$$

A nucleus–nucleus collision is accepted if at least one such nucleon–nucleon collision was obtained.

The values used for σ_{NN} are usually obtained from the difference of total and elastic pp cross section measurements [17–21], or interpolated using fits performed by the COMPETE Collaboration [22] as shown in Fig. 1. Common values are summarized in Tab. II for a number of collision energies, and in good agreement with the COMPETE fits. At 13 TeV, however, the preliminary data [23, 24] indicate that the fit is overpredicting the cross section by about 15% and, hence, 78 mb, which is between the central value of the data and the fit, and roughly within 1σ of the experimental uncertainty, is used in the paper.

To estimate systematic uncertainties for calculated quantities it is suggested to systematically modify the parameters of the calculation [13]. One typically varies the parameters of the nuclear density profile within the measured 1σ uncertainties, the minimum inter-nucleon separation distance by 100%, and the σ_{NN} by about ± 3 mb and ± 5 mb at RHIC and LHC, respectively.

The Glauber calculation gives $\sigma_{\text{PbPb}}^{\text{MC}} = 7.6 \pm 0.2$ b and $\sigma_{\text{pPb}}^{\text{MC}} = 2.1 \pm 0.1$ b for the total PbPb and pPb cross

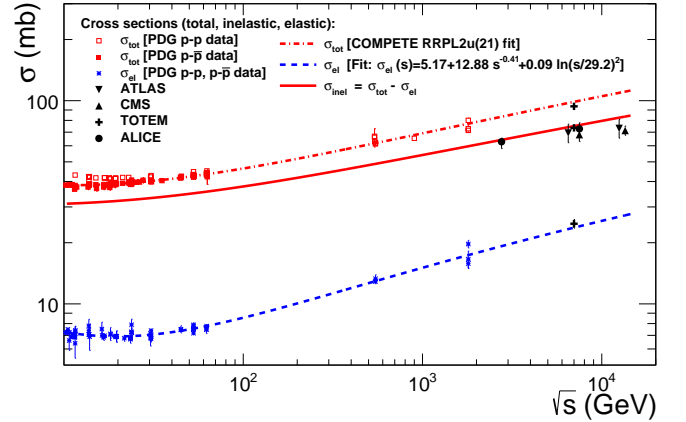


FIG. 1: Available data of total, elastic and inelastic cross sections measured in pp and $p\bar{p}$ collisions [17–21]. The data [23, 24] at 13 TeV are preliminary. The curves are fits performed by the COMPETE Collaboration [22].

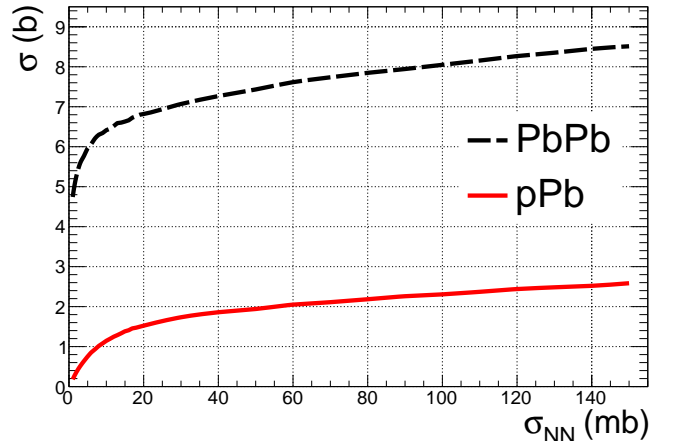


FIG. 2: Calculated total cross sections for PbPb and pPb collisions as a function of σ_{NN} .

sections, in good agreement with the measured values of $\sigma_{\text{PbPb}} = 7.7 \pm 0.6$ b at $\sqrt{s_{\text{NN}}} = 2.76$ TeV [25] and $\sigma_{\text{pPb}} = 2.06 \pm 0.08$ b at $\sqrt{s_{\text{NN}}} = 5.02$ TeV [26], respectively. For PbPb at $\sqrt{s_{\text{NN}}} = 5.02$ a total cross section of $\sigma_{\text{PbPb}}^{\text{MC}} = 7.7 \pm 0.2$ b is predicted. The total cross sections of PbPb and pPb as a function of σ_{NN} are shown in Fig. 2 calculated using the central values of the parameters (i.e. without systematic uncertainties, which would be about 3 and 8%, respectively).

MC Glauber calculations are typically used to compute geometrical properties of the collision, such as the number of participating nucleons in the collision, N_{part} , i.e. the number of nucleons that are hit at least once, or the number of independent nucleon–nucleon collisions, N_{coll} , i.e. the total number of collisions between nucleons. Particle production at low p_{T} roughly scales with N_{part} [27], while hard processes in absence of strong final state modification scale with N_{coll} [28–30]. Examples of geometri-

¹ The reaction plane, i.e. the plane defined by the impact parameter and the beam direction, is given by the x - and z -axes, while the transverse plane is given by the x - and y -axes.

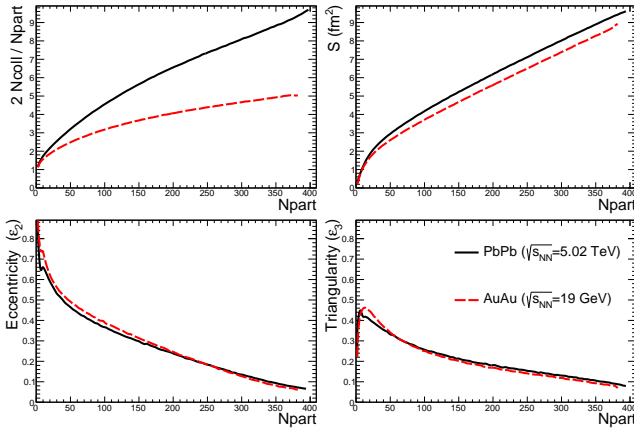


FIG. 3: Geometric properties computed with Glauber MC for AuAu collisions at $\sqrt{s_{NN}} = 19$ GeV and PbPb collisions at $\sqrt{s_{NN}} = 5.02$ TeV.

cal properties are shown in Fig. 3. The ratio between $N_{\text{coll}}/N_{\text{part}}$ normalized to that of pp (i.e. 1/2), which has been argued to be a measure for the relative importance of hard versus soft processes, rises with centrality and in particular with collision energy. The overlap area of the two colliding nuclei is proportional to $S = \sqrt{\sigma_x^2 \sigma_y^2 - \sigma_{xy}^2}$, given by the (co-)variances of the participant distributions in the transverse plane [13]. The area can also be directly computed from the MC as explained in App. B, leading to a slightly different shape.

The eccentricity [31] and triangularity [32] of the collision region, given by $\epsilon_i = \langle r^i \cos(i\phi - i\psi_i) \rangle / \langle r^i \rangle$ (for $i = 2$ and 3, respectively) [33], are used to characterize the initial geometrical shape. These properties are similar between AuAu and PbPb collisions, and at different energies.

III. EXTENSION TO SUB-NUCLEON LEVEL

The calculation can be readily extended to sub-nucleon level by assuming that a nucleon carries N_c degrees of freedom. Often $N_c = 3$ for three constituent quarks [6–8], but larger numbers (up to $N_c = 17$) have previously [34] been used to account for the effective number of partonic degrees of freedom. Generalizing Eq. 2, the interaction between two constituents can be modeled by an effective parton–parton cross section (σ_{cc}) in the same way as before, i.e. two constituents from different nuclei collide if their relative transverse distance is less than

$$D = \sqrt{\sigma_{cc}/\pi}. \quad (3)$$

There are two, somewhat limiting, cases to distribute sub-nucleon degrees of freedom. The first is to bind constituents to nucleons making up the nucleus (labeled as “bound” in figures). In this case, N_c constituents are ra-

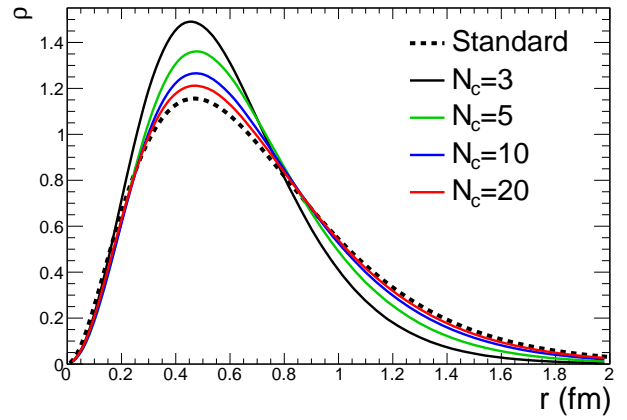


FIG. 4: Radial distribution of constituents after recentering when constructed from the standard parameterization (Eq. 4) for different N_c .

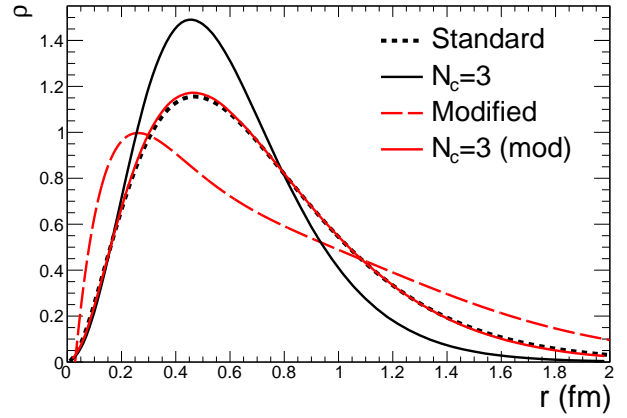


FIG. 5: Radial distribution of constituents after recentering when constructed from the standard (Eq. 4) or modified (Eq. 5) parameterizations for $N_c = 3$.

dially distributed centered around each nucleon according to

$$\rho(r) = \exp(-r/R) \quad (4)$$

with $R = 0.234$ fm based on the measured form factor of the proton [35]. The second is to freely distribute constituents over the whole nucleus (labeled as “free” in figures). In this case $A \times N_c$ constituents are distributed according to Eq. 1.² In both cases, a hard core repulsion potential is not considered.

When the constituents are bound to nucleons, recentering of the constituents to align with the centers of their respective nucleons, introduces a distortion of the resulting radial constituent distribution. The effect is

² This is conceptually similar to the optical approach originally used in Ref. [6].

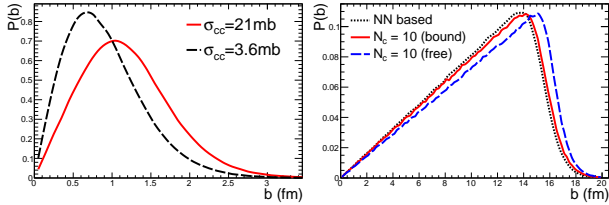


FIG. 6: Impact parameter distribution for pp (left) and PbPb (right) collisions. In case of pp, $\sigma_{cc} = 3.6$ and 21 mb with $N_c = 3$ are used for pp collisions at $\sqrt{s} = 0.2$ and 7 TeV, respectively. For PbPb collisions at $\sqrt{s_{NN}} = 5.02$ TeV, the standard nucleon-based approach is compared to bound and freely-distributed cases using $\sigma_{cc} = 3$ mb and $N_c = 10$.

most dramatic for $N_c = 3$, and reduces quickly with increasing number of constituents as shown in Fig. 4. For $N_c = 3$, the distortion can be avoided by distributing the constituents according to an empirically determined function [36]

$$\rho(r) = r^2 \exp(-r/R) \times [(1.22 - 1.89r + 2.03r^2) (1 + 1/r - 0.03/r^2)(1 + 0.15r)] \quad (5)$$

as shown in Fig. 5. Equation 5 holds for $N_c = 3$. Hence, it is used as an alternative to Eq. 4 only in the case of constraining constituents to nucleons. This case is labeled as “mod” when displayed in figures. If not otherwise specified in the following, we do not recenter the constituents. In any case, not recentering has a negligible effect on the center of a nucleus since the deviations from the center-of-mass average out over AN_c degrees of freedom.

The resulting impact parameter distributions differ from a straight line ($\propto b$) which holds in the case of a hard-sphere profile. Examples are shown in Fig. 6 for pp collisions at $\sqrt{s} = 0.2$ and 7 TeV in the left, and for PbPb collisions at $\sqrt{s_{NN}} = 5.02$ TeV in the right panel. In the case of pp, the distributions are obtained using $\sigma_{cc} = 21$ and 3.6 mb for $N_c = 3$, and extend beyond the hard-sphere limit of about 1.0 and 1.5 fm, respectively. In the case of PbPb, the distribution obtained for the standard NN based approach is compared to the bound and freely-distributed cases for $\sigma_{cc} = 3$ mb and $N_c = 10$. Freely-distributing constituents instead of binding them into nucleons generally leads to a wider impact parameter distribution.

Nuclear reaction cross sections can be computed by counting if there was at least one collision among two constituents. Figure 7 shows the dependence of σ_{NN} on σ_{cc} for various choices of N_c . As expected, σ_{NN} strongly increases with increasing σ_{cc} and N_c . For $N_c = 3$, the two parameterizations lead to a small but noticeable difference on σ_{NN} for $\sigma_{cc} \gtrsim 10$ mb. Figure 8 shows the increase of the PbPb (top) and pPb (bottom) cross sections with σ_{cc} for different values of N_c and the two ways to distribute the constituents, e.g. bound to nucleons or freely distributed inside the nucleus. For the same pa-

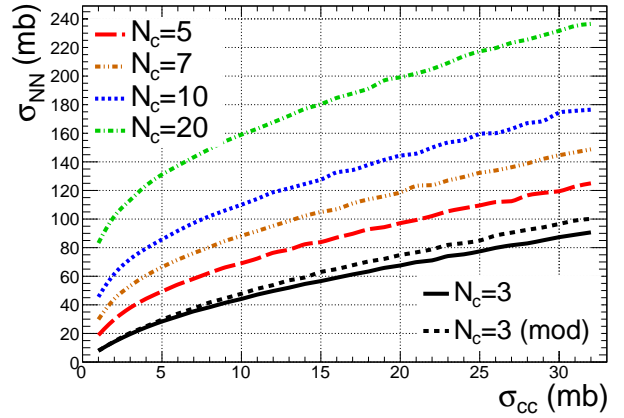


FIG. 7: Calculated σ_{NN} for various choices of N_c versus σ_{cc} .

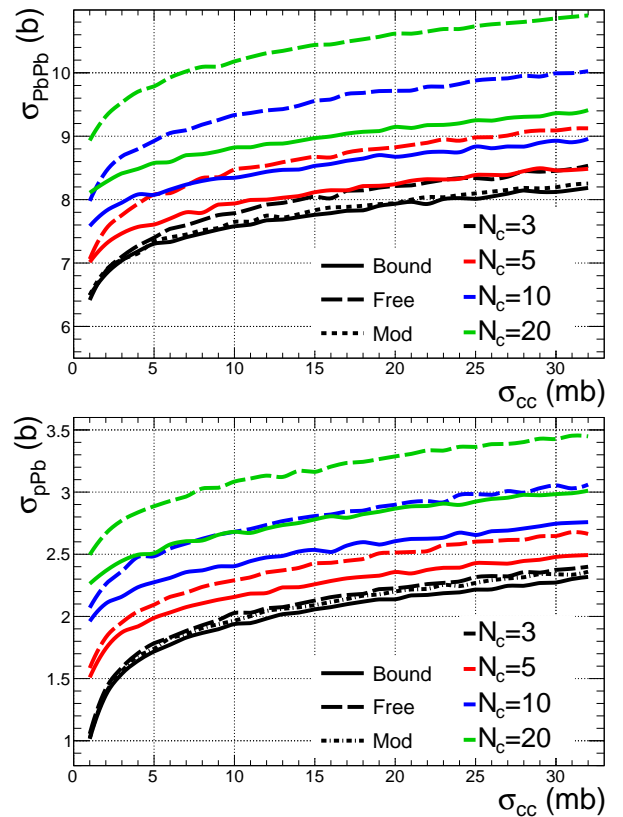


FIG. 8: Calculated total cross section for PbPb (top) and pPb (bottom) collisions for various choices of N_c versus σ_{cc} for the bound and free cases.

rameters, the freely-distributing case always leads to a larger cross section than the bound case. In particular, for large σ_{cc} and N_c the likelihood for peripheral collisions to occur increases significantly, making the total cross section exceed the value expected from geometrical considerations (also visible in the right panel of Fig. 6). For example, 8 b corresponds to an effective radius of about 8 fm (which is larger than $R + 2a$ of Pb).

N_c	σ_{cc} (mb)	μ	ν	σ_{NN} (mb)	σ_{PbPb} (b)	$\sigma_{PbPb}^{\text{free}}$ (b)
3	18	3.4	2.6	63.3	7.83	8.15
3*	18	3.2	2.3	70.3	7.90	
5	10	4.3	3.6	69.1	7.94	8.47
7	5.5	4.8	3.9	69.0	7.92	8.52
10	3	5.4	4.2	72.1	7.95	8.68
3	14.4	3.3	2.3	55.4	7.74	
3*	11.9	3.0	2.0	53.6	7.71	
3	8.8	3.0	1.9	40.9		7.74
5	6.4	3.9	2.8	55.8	7.75	
5	2.9	3.1	1.9	37.2		7.76
10	1.7	4.4	2.9	56.8	7.78	

TABLE III: Values for PbPb collisions at $\sigma_{NN} = 5.02$ TeV. Input parameters are N_c , σ_{cc} and the way the constituents are distributed (bound, modified and free). Output values are $\mu = \langle N_{\text{cpart}} \rangle$, $\nu = \langle N_{\text{coll}} \rangle$, σ_{NN} and σ_{PbPb} as well as $\sigma_{PbPb}^{\text{free}}$ for the freely distributing case. The modified cases are indicated with *. The parameters in rows above the horizontal line attempt to match $\sigma_{NN} = 70$ mb, while those below the horizontal line to match $\sigma_{PbPb} = 7.7$ b.

N_c	σ_{cc} (mb)	μ	ν	σ_{NN} (mb)	σ_{AuAu} (b)	$\sigma_{AuAu}^{\text{free}}$ (b)
3	6	2.7	1.7	31.9	6.89	7.01
3*	6	2.6	1.6	33.9	6.91	
5	2.5	3.0	1.8	33.9	7.01	7.16
3	3.6	2.5	1.4	22.4	6.65	
3*	3.8	2.5	1.4	24.1	6.67	
3	3.2	2.5	1.4	20.5		6.66
5	1.4	2.6	1.5	23.2	6.70	

TABLE IV: Values for AuAu collisions at $\sigma_{NN} = 19.6$ TeV, with $\sigma_{NN} = 33$ mb and $\sigma_{AuAu} = 6.7$ b. See description in Tab. III for more information.

In the following section, results will be discussed where the parameters for the calculation are chosen to approximately reflect PbPb collisions at $\sqrt{s_{NN}} = 5.02$ TeV, and AuAu collisions at $\sqrt{s_{NN}} = 19.6$ GeV, respectively. The calculations are performed for various choices of N_c and σ_{cc} , as well as various ways to distribute the constituents, i.e. bound, modified and free cases. The parameters, which are summarized in Tab. III and Tab. IV, have been set to roughly match the corresponding σ_{NN} and the total σ_{PbPb} , respectively.

IV. RESULTS

In this section, results of constituent Glauber model calculations are presented for various input parameters and collision systems.

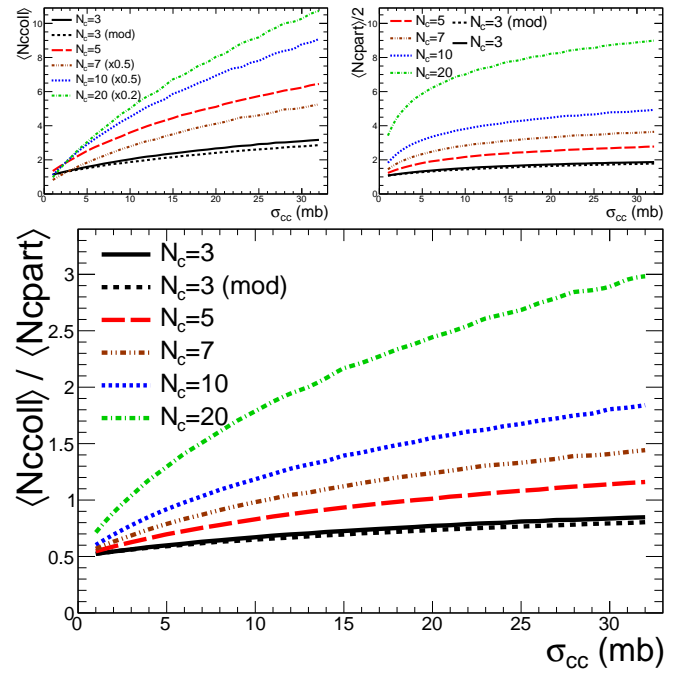


FIG. 9: Average values of N_{coll} (top left) and N_{cpart} (top right panel), as well as of the ratio $N_{\text{coll}}/N_{\text{cpart}}$ (bottom panel) versus σ_{cc} for various N_c in pp collisions.

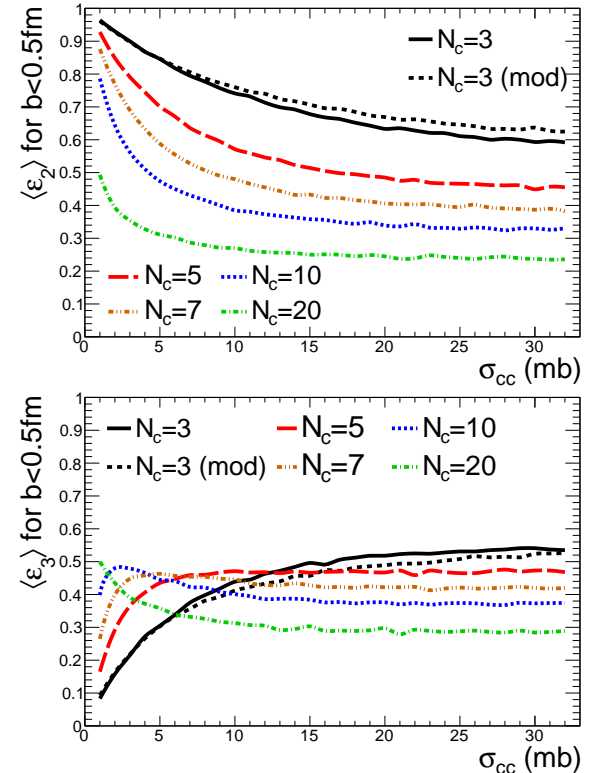


FIG. 10: Average eccentricity (top) and triangularity (bottom) for $b < 0.5$ fm versus σ_{cc} for various N_c in pp collisions.

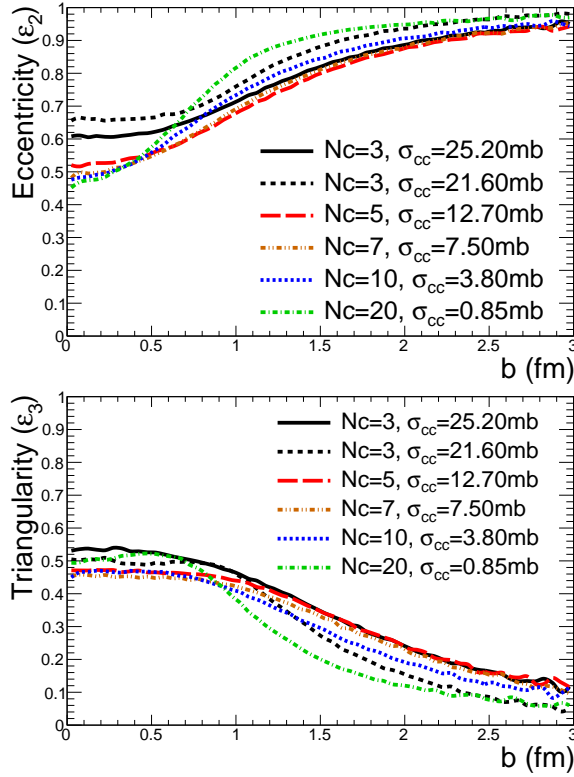


FIG. 11: Eccentricity (top) and Triangularity (bottom) versus b for various N_c in pp collisions at 13 TeV. The calculation for $\sigma_{cc} = 21.60$ mb corresponds to the modified case.

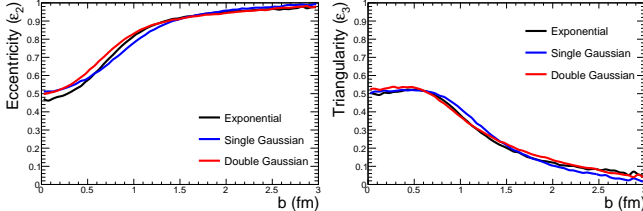


FIG. 12: Eccentricity (left) and triangularity (right) versus b for $N_c = 20$ and $\sigma_{cc} = 0.85$ mb corresponding to pp collisions at 13 TeV using Exponential, Single and Double Gaussian density profiles (see text).

A. pp collisions

Figure 9 shows average values of N_{coll} and N_{cpart} , as well as of the ratio $N_{\text{coll}}/N_{\text{cpart}}$ versus σ_{cc} for various N_c in pp collisions. The resulting values increase with increasing N_c and σ_{cc} compared to those at nucleon level, which are $N_{\text{part}} = 2$, $N_{\text{coll}} = 1$, and $N_{\text{coll}}/N_{\text{part}} = 0.5$.

Figure 10 shows the dependence of the average eccentricity $\langle \varepsilon_2 \rangle$ and triangularity $\langle \varepsilon_3 \rangle$ versus σ_{cc} for various N_c in central pp collisions with $b < 0.5$ fm. Increasing N_c and σ_{cc} decreases the observed initial-state anisotropy as expected for a spherically symmetric system. In the

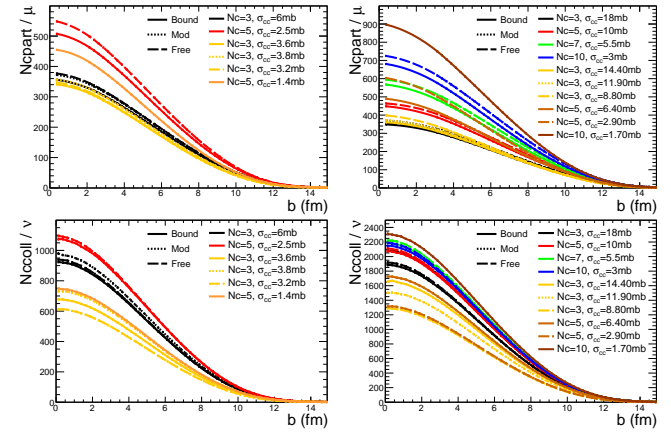


FIG. 13: N_{cpart}/μ (top) and N_{coll}/ν (bottom panels) for AuAu (left) and PbPb (right panels) collisions. The parameters for the calculations are summarized in Tab. III and Tab. IV.

limiting case, without sub-structure, $\varepsilon_2 = 1$ and $\varepsilon_3 = 0$. Figure 11 shows eccentricity and triangularity versus b for a set of input parameters reflecting pp collisions at 13 TeV. For central collisions ($b < 0.5$ fm) $0.45 < \varepsilon_2 < 0.65$ and $0.46 < \varepsilon_3 < 0.54$ leading to scaled values of about 0.1 and 0.02 for measured values [37, 38] of $v_2 \sim 0.05$ and $v_3 \sim 0.01$, respectively. Figure 12 compares eccentricity and triangularity versus b for $N_c = 20$ and $\sigma_{cc} = 0.85$ mb corresponding to pp collisions at 13 TeV for different density profiles. The first is the exponential (Eq. 4) profile, used so far. The others are Single and Double Gaussian profiles, implemented in the impact-parameter dependent Glauber-like collision framework of PYTHIA8 [39], and used to model multi-parton interactions. The resulting distributions for ε_2 and ε_3 do not differ from the standard case.

B. AA collisions

The results for AA collisions, discussed in this section, are obtained for calculations where the parameters are chosen to approximately reflect PbPb collisions at $\sqrt{s_{\text{NN}}} = 5.02$ TeV, and AuAu collisions at $\sqrt{s_{\text{NN}}} = 19.6$ GeV, respectively. The parameters are summarized in Tab. III for PbPb and Tab. IV for AuAu collisions.

Figure 13 shows N_{cpart}/μ and N_{coll}/ν versus b , where $\mu = \langle N_{\text{cpart}} \rangle$ and $\nu = \langle N_{\text{coll}} \rangle$ in pp collision, respectively. Figure 14 shows the ratio $N_{\text{cpart}}/N_{\text{part}}$ versus N_{part} normalized to $\mu/2$. The calculations are performed in small bins of b and then matched to the corresponding N_{part} at nucleon level, since in peripheral events $\langle N_{\text{part}} \rangle$ for events selected with $N_{\text{cpart}} > 0$ slightly differs from those calculated at nucleon level and selected with $N_{\text{part}} > 0$. In particular for $N_c \leq 5$, the shape is similar to that of the measured $2dN/d\eta/N_{\text{part}}$ [27, 40, 41]. The inverse of what is plotted, i.e. $\mu/2N_{\text{part}}/N_{\text{cpart}}$, would be the

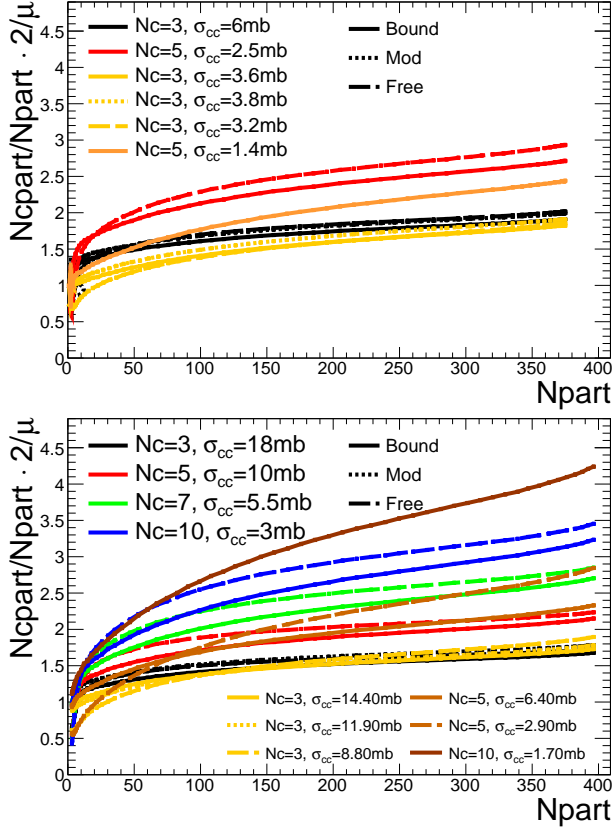


FIG. 14: Ratio $N_{\text{cpart}}/N_{\text{part}}$ normalized to $\mu/2$ for AuAu (top) and PbPb (bottom panel) collisions. The parameters for the calculations are summarized in Tab. III and Tab. IV.

factor needed to translate the measurements scaled by $N_{\text{part}}/2$ to N_{cpart}/μ . Hence, the correction would affect the shape the strongest for peripheral events, making $\mu dN/d\eta/N_{\text{cpart}}$ approximately flat.

Indeed, this is directly demonstrated in Fig. 15, which shows $dN/d\eta$ in PbPb collisions at $\sqrt{s_{\text{NN}}} = 17.2$ GeV [42] and $\sqrt{s_{\text{NN}}} = 5.02$ TeV [41] scaled by N_{cpart}/μ for sub-nucleon ($N_c > 1$) and $N_{\text{part}}/2$ for nucleon ($N_c = 1$) participants. Using $N_c = 3$ and $N_c = 5$ for $\sqrt{s_{\text{NN}}} = 17.2$ GeV and 5.02 TeV, respectively, approximately flatten the scaled data, which when fit with a first order polynomial exhibit a slope consistent with 0 (0.0002 ± 0.0004 and 0.0000 ± 0.0002 , respectively). For the 5.02 TeV data also the cases $N_c = 3$ and 7 are shown, which exhibit a small positive (of 0.0016 ± 0.0004) and negative (-0.0009 ± 0.0003) slope, respectively. This may be an indication that the effective partonic degrees of freedom relevant for soft particle production are on average about 5 at high energy, and about 3 at lower collision energy.

This is further investigated by comparing particle production in central AA to pp collision data. The mid-rapidity $dN/d\eta$ in central AA collisions scaled by N_{part} compared to that in inelastic pp collisions turned out to rise stronger with collision energy, with $s_{\text{NN}}^{0.155}$ rather

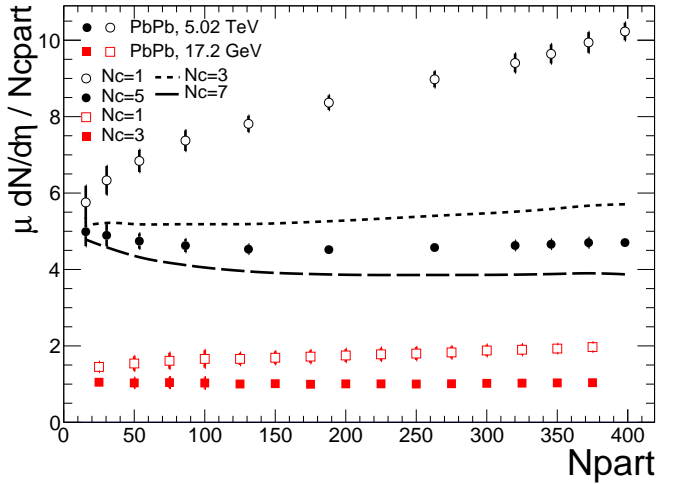


FIG. 15: Values of $dN/d\eta$ in PbPb collisions at $\sqrt{s_{\text{NN}}} = 17.2$ GeV and $\sqrt{s_{\text{NN}}} = 5.02$ TeV scaled by N_{cpart}/μ for sub-nucleon ($N_c > 1$) and $N_{\text{part}}/2$ for nucleon ($N_c = 1$) participants. The data are from [41, 42], drawn with only point-to-point uncorrelated systematic uncertainties. The 17.2 GeV data are scaled using $N_c = 3$ ($\sigma_{\text{cc}} = 6$ mb). The 5.02 TeV data are scaled using $N_c = 5$ ($\sigma_{\text{cc}} = 10$ mb). The lines show the central points if the data were scaled by $N_c = 3$ ($\sigma_{\text{cc}} = 18$ mb, modified profile) and $N_c = 7$ ($\sigma_{\text{cc}} = 5.5$ mb), respectively.

than $s_{\text{NN}}^{0.103}$, respectively [41]. To evaluate if normalizing by constituent instead of nucleon participants would lead to a more similar behavior, the ratio N_{cpart}/μ has been computed for various N_c and several ways to distribute the sub-nuclear degrees of freedom. The computed ratios for $b < 3.5$ fm are shown versus $\sqrt{s_{\text{NN}}}$ in Fig. 16, and found to slightly decrease with increasing $\sqrt{s_{\text{NN}}}$. This trend can be compared to data, using the ratio of the power-law fits to the central AA and the inelastic pp data taken from Ref. [41]. The ratio of the power-law fits is scaled by 160 to roughly account for normalizing the central AA data by $N_{\text{part}}/2$, since for central AuAu at $\sqrt{s_{\text{NN}}} = 19.6$ GeV $N_{\text{part}} \approx 340$, while $N_{\text{part}} \approx 385$ for PbPb at $\sqrt{s_{\text{NN}}} = 5.02$ TeV. As can be seen in the figure, the data exhibit a different trend, i.e. the ratio is slightly rising with $\sqrt{s_{\text{NN}}}$. The comparison between data and calculations does not reveal a preferred constant value for N_c . Instead, at lower energy $N_c = 3$, while at higher energy $N_c = 5$ is supported by the data, indicating that the number of relevant partonic degrees of freedom increase with increasing collision energy. On an absolute scale, Figure 17 indeed confirms that scaling with N_{cpart}/μ for $N_c = 3$ or 5 leads to a more similar collision energy dependence of central AA and inelastic pp data than based on N_{part} (labeled with $N_c = 1$). In particular, it is important to realize that while the collision energy varies by 3 orders of magnitude, the scaled $dN/d\eta$ only changes by a factor 2.

Figure 18 shows the eccentricity and triangularity versus N_{part} calculated for parameters given in Tab. III and

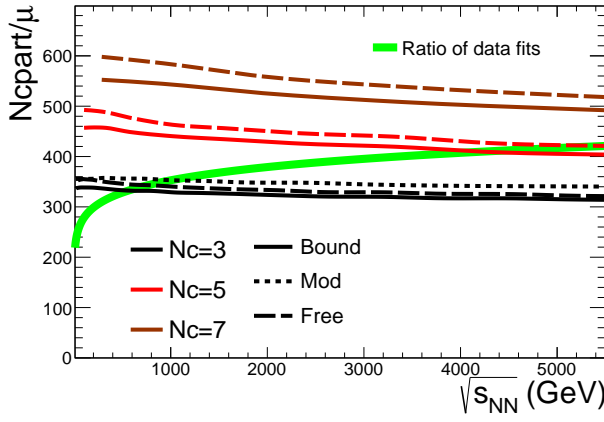


FIG. 16: Ratio of fits to central AA (scaled by 160 to approximately account for $N_{\text{part}}/2$) and inelastic pp collisions compared to N_{cpart}/μ from constituent Glauber calculations for $b < 3.5$ fm. The values for the power law fits are taken from [41].

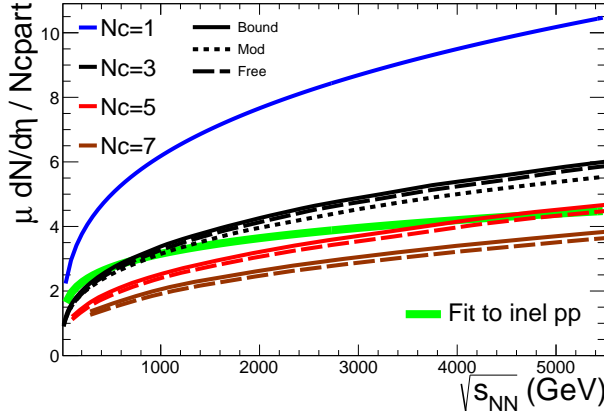


FIG. 17: Power-law fit of $dN/d\eta$ from inelastic pp collisions compared to scaled central AA data. The AA curves are obtained from a power-law fit to $2dN/d\eta/N_{\text{part}}$ scaled by μ/N_{cpart} (multiplied by 160 to approximately account for $N_{\text{part}}/2$) for constituent Glauber calculations with $b < 3.5$ fm. In the case of $N_c = 1$, $N_{\text{cpart}} = N_{\text{part}}$ and $\mu = 2$, the shown curve essentially represents the original fit to $2dN/d\eta/N_{\text{part}}$. The values for the power law fits are taken from [41].

Tab. IV, and are quite similar to those calculated from participant nucleons, as also concluded in Ref. [43]. The triangularity exhibits a stronger variation to changes of the calculation than the eccentricity, which is found to be quite insensitive to the actual values of the parameters. As in the case of the nucleon participant calculation, ε_3 is only up to 10–20% larger than ε_2 in ultra-central collisions, which can not resolve the question why the measured $v_2\{2\} \approx v_3\{2\}$ in ultra-central collisions [44, 45].

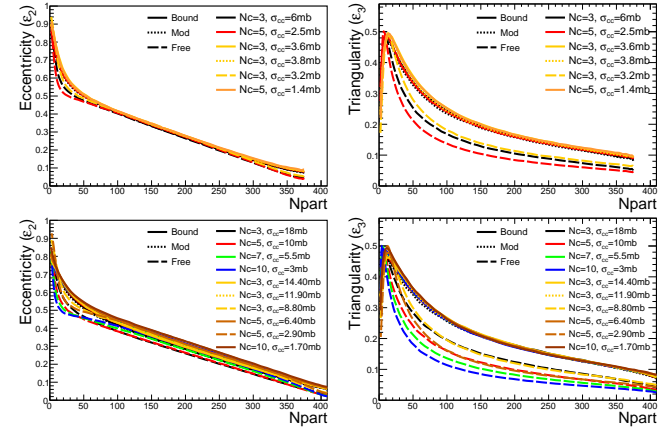


FIG. 18: Eccentricity (left) and triangularity (right panels) for AuAu (top) and PbPb (bottom panels) collisions. The parameters for the calculations are summarized in Tab. III and Tab. IV.

V. SUMMARY

Glauber models based on nucleon–nucleon interactions are commonly used to calculate properties of the initial state in high-energy nuclear collisions, and their dependence on impact parameter or number of participating nucleons. In this article, an extension to the Glauber model is presented, which accounts for an arbitrary number of effective sub-nucleon degrees of freedom, or partonic constituents, in the nucleons. Properties of the initial state, such as the number of constituent participants and collisions, as well as eccentricity and triangularity, are calculated and systematically compared for different assumptions to distribute the sub-nuclear degrees of freedom and for various collision systems. It is demonstrated that at high collision energy the number of produced particles scales with an average number of sub-nucleon degrees of freedom of between 3 and 5. As in the case of the nucleon participant calculation, ε_3 is only up to 10–20% larger than ε_2 in ultra-central collisions, which can not resolve the question why the measured $v_2\{2\} \approx v_3\{2\}$ in ultra-central collisions. The code for the constituent Monte Carlo Glauber program is made publicly available. The author welcomes comments on the code and suggestions on how to make it more useful to both experimentalists and theorists.

Acknowledgments

I would like to thank J.Schukraft and S.Sorensen for interesting discussions. This work is supported in part by the U.S. Department of Energy, Office of Science, Office of Nuclear Physics, under contract number DE-AC02-05CH11231.

[1] M. L. Miller, K. Reygers, S. J. Sanders, and P. Steinberg, Ann. Rev. Nucl. Part. Sci. **57**, 205 (2007), [arXiv:nucl-ex/0701025](https://arxiv.org/abs/nucl-ex/0701025).

[2] A. Bialas, M. Bleszynski, and W. Czyz, Nucl. Phys. **B111**, 461 (1976).

[3] K. J. Eskola, K. Kajantie, and J. Lindfors, Nucl. Phys. **B323**, 37 (1989).

[4] B. Alver, M. Baker, C. Loizides, and P. Steinberg (2008), [arXiv:0805.4411](https://arxiv.org/abs/0805.4411).

[5] M. Rybczynski, G. Stefanek, W. Broniowski, and P. Bozek, Comput. Phys. Commun. **185**, 1759 (2014), [arXiv:1310.5475](https://arxiv.org/abs/1310.5475).

[6] S. Eremin and S. Voloshin, Phys. Rev. **C67**, 064905 (2003), [arXiv:nucl-th/0302071](https://arxiv.org/abs/nucl-th/0302071).

[7] S. S. Adler et al. (PHENIX), Phys. Rev. **C89**, 044905 (2014), [arXiv:1312.6676](https://arxiv.org/abs/1312.6676).

[8] A. Adare et al. (PHENIX), Phys. Rev. **C93**, 024901 (2016), [arXiv:1509.06727](https://arxiv.org/abs/1509.06727).

[9] R. A. Lacey, P. Liu, N. Magdy, M. Csanad, B. Schweid, N. N. Ajitanand, J. Alexander, and R. Pak (2016), [arXiv:1601.06001](https://arxiv.org/abs/1601.06001).

[10] L. Zheng and Z. Yin, Eur. Phys. J. **A52**, 45 (2016), [arXiv:1603.02515](https://arxiv.org/abs/1603.02515).

[11] C. Loizides (2016), [arXiv:1602.09138](https://arxiv.org/abs/1602.09138).

[12] P. Bozek, W. Broniowski, and M. Rybczynski (2016), [arXiv:1604.07697](https://arxiv.org/abs/1604.07697).

[13] B. Alver et al., Phys. Rev. **C77**, 014906 (2008), [arXiv:0711.3724](https://arxiv.org/abs/0711.3724).

[14] H. De Vries, C. W. De Jager, and C. De Vries, Atom. Data Nucl. Data Tabl. **36**, 495 (1987).

[15] Q. Y. Shou, Y. G. Ma, P. Sorensen, A. H. Tang, F. Videbæk, and H. Wang, Phys. Lett. **B749**, 215 (2015), [arXiv:1409.8375](https://arxiv.org/abs/1409.8375).

[16] C. Loizides, J. Nagle, and P. Steinberg (2014), [arXiv:1408.2549](https://arxiv.org/abs/1408.2549).

[17] K. A. Olive et al. (Particle Data Group), Chin. Phys. **C38**, 090001 (2014).

[18] G. Aad et al. (ATLAS), Nature Commun. **2**, 463 (2011), [arXiv:1104.0326](https://arxiv.org/abs/1104.0326).

[19] G. Antchev et al. (TOTEM), Europhys. Lett. **96**, 21002 (2011), [arXiv:1110.1395](https://arxiv.org/abs/1110.1395).

[20] S. Chatrchyan et al. (CMS), Phys. Lett. **B722**, 5 (2013), [arXiv:1210.6718](https://arxiv.org/abs/1210.6718).

[21] B. Abelev et al. (ALICE), Phys. Rev. **C88**, 044909 (2013), [arXiv:1301.4361](https://arxiv.org/abs/1301.4361).

[22] J. R. Cudell, V. V. Ezhela, P. Gauron, K. Kang, Yu. V. Kuyanov, S. B. Lugovsky, E. Martynov, B. Nicolescu, E. A. Razuvaev, and N. P. Tkachenko (COMPETE), Phys. Rev. Lett. **89**, 201801 (2002), [arXiv:hep-ph/0206172](https://arxiv.org/abs/hep-ph/0206172).

[23] A. Collaboration (ATLAS) (2015).

[24] C. Collaboration (CMS) (2016).

[25] B. Abelev et al. (ALICE), Phys. Rev. Lett. **109**, 252302 (2012), [arXiv:1203.2436](https://arxiv.org/abs/1203.2436).

[26] V. Khachatryan et al. (CMS) (2015), [arXiv:1509.03893](https://arxiv.org/abs/1509.03893).

[27] B. Alver et al. (PHOBOS), Phys. Rev. **C83**, 024913 (2011), [arXiv:1011.1940](https://arxiv.org/abs/1011.1940).

[28] M. M. Aggarwal et al. (WA98), Phys. Rev. Lett. **85**, 3595 (2000), [arXiv:nucl-ex/0006008](https://arxiv.org/abs/nucl-ex/0006008).

[29] S. S. Adler et al. (PHENIX), Phys. Rev. Lett. **94**, 232301 (2005), [arXiv:nucl-ex/0503003](https://arxiv.org/abs/nucl-ex/0503003).

[30] S. Chatrchyan et al. (CMS), Phys. Lett. **B710**, 256 (2012), [arXiv:1201.3093](https://arxiv.org/abs/1201.3093).

[31] B. Alver et al. (PHOBOS), Phys. Rev. Lett. **98**, 242302 (2007), [arXiv:nucl-ex/0610037](https://arxiv.org/abs/nucl-ex/0610037).

[32] B. Alver and G. Roland, Phys. Rev. **C81**, 054905 (2010), [Erratum: Phys. Rev. C82, 039903(2010)], [arXiv:1003.0194](https://arxiv.org/abs/1003.0194).

[33] D. Teaney and L. Yan, Phys. Rev. **C83**, 064904 (2011), [arXiv:1010.1876](https://arxiv.org/abs/1010.1876).

[34] D. d'Enterria, G. K. Eyyubova, V. L. Korotkikh, I. P. Lokhtin, S. V. Petrushanko, L. I. Sarycheva, and A. M. Snigirev, Eur. Phys. J. **C66**, 173 (2010), [arXiv:0910.3029](https://arxiv.org/abs/0910.3029).

[35] R. Hofstadter, Rev. Mod. Phys. **28**, 214 (1956).

[36] J. T. Mitchell, D. V. Perepelitsa, M. J. Tannenbaum, and P. W. Stankus (2016), [arXiv:1603.08836](https://arxiv.org/abs/1603.08836).

[37] G. Aad et al. (ATLAS) (2015), [arXiv:1509.04776](https://arxiv.org/abs/1509.04776).

[38] V. Khachatryan et al. (CMS), CMS-PAS-FSQ-15-002 (2015).

[39] R. Corke and T. Sjostrand, JHEP **05**, 009 (2011), [arXiv:1101.5953](https://arxiv.org/abs/1101.5953).

[40] K. Aamodt et al. (ALICE), Phys. Rev. Lett. **106**, 032301 (2011), [arXiv:1012.1657](https://arxiv.org/abs/1012.1657).

[41] J. Adam et al. (ALICE) (2015), [arXiv:1512.06104](https://arxiv.org/abs/1512.06104).

[42] S. S. Adler et al. (PHENIX), Phys. Rev. **C71**, 034908 (2005), [Erratum: Phys. Rev. C71, 049901(2005)], [arXiv:nucl-ex/0409015](https://arxiv.org/abs/nucl-ex/0409015).

[43] M. Miller and R. Snellings (2003), [arXiv:nucl-ex/0312008](https://arxiv.org/abs/nucl-ex/0312008).

[44] C. Shen, Z. Qiu, and U. Heinz, Phys. Rev. **C92**, 014901 (2015), [arXiv:1502.04636](https://arxiv.org/abs/1502.04636).

[45] C. Shen and U. Heinz (2015), [arXiv:1507.01558](https://arxiv.org/abs/1507.01558).

[46] R. Brun and F. Rademakers, Nucl. Instrum. Meth. **A389**, 81 (1997).

[47] J. D. Bjorken, Phys. Rev. **D27**, 140 (1983).

Appendix A: Program code

The program code, called “runCGM.C”, for the generalized constituent Monte Carlo Glauber can be found at <http://tglaubermc.hepforge.org/svn/branches/tools/runCGM.C>. It requires “runglauber_v2.3.C” from the most recent TGlauberMC version (v2.3) [16], which can be downloaded from HepForge (<http://www.hepforge.org/downloads/tglaubermc>), and ROOT [46] (see <http://root.cern.ch> for installation files and documentation.). To compile the code, execute at the ROOT prompt:

```
.L runglauber_2.3.C+
.L runCGM.C+
```

The function “runCGM” can be run with the following arguments:

```
Int_t n          = number of events
const char *sysA = system A
const char *sysB = system B
Double_t signn  = NN cross section (mb)
```

```

Double_t mind      = min. dist. betw. nucleons
Int_t nc          = number of constituents / dof
Double_t sigcc    = constituent cross section (mb)
Int_t type,       -> how to distribute dof:
                     =0 no recentering
                     =5 modified (PHENIX)
                     =8 free no recentering
const char *fname = output filename
Double_t bmin     = min. imp. parameter
Double_t bmax     = max. imp. parameter

```

The output ROOT “ntuple” contains the following list of per-event variables:

```

Npart   = number of nucleon participants
Ncoll   = number of nucleon collisions
B       = impact parameter
Ncpart  = number of constituent participants
Nccoll  = number of constituent collisions
Ap      = area def. by participant (co-)variances
Ac      = area def. by constituent (co-)variances
EccXP  = eccX nucleon participants (X=1-5)
EccXC  = eccX constituent participants (X=1-5)

```

All distributions discussed in Sec. IV have been obtained from the output of “runGCM”.

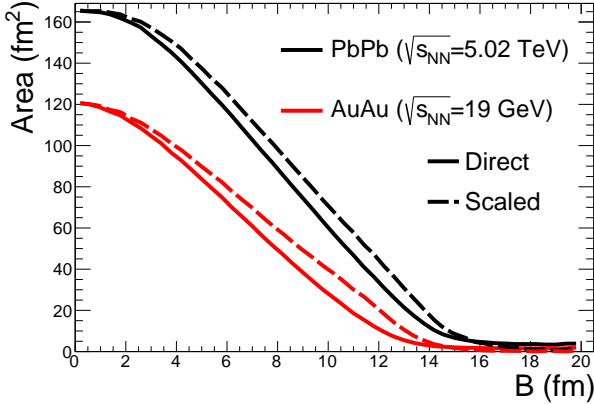


FIG. 19: Area calculated directly by counting of the overlap area and scaled using the participant widths for AuAu collisions at $\sqrt{s_{NN}} = 19$ GeV and PbPb collisions at $\sqrt{s_{NN}} = 5.02$ TeV.

Appendix B: Area calculation

As briefly mentioned in Sec. II, the overlap area of two colliding nuclei is usually taken to be proportional to

$S = \sqrt{\sigma_x^2 \sigma_y^2 - \sigma_{xy}^2}$, given by the (co-)variances of the participant distributions in the transverse plane [13]. However, using the participant distributions does not provide a direct measure of the area, and in particular misses also the absolute normalization. Instead, one can event-by-event compute the overlap area directly using a fine-grained grid. Figure 19 compares the two approaches for AuAu collisions at $\sqrt{s_{NN}} = 19$ GeV and PbPb collisions at $\sqrt{s_{NN}} = 5.02$ TeV, where the results using the participant widths were rescaled by A_0/S_0 where S_0 and the absolute area A_0 were obtained at $b = 0$ fm. The values are $S_0 = 9.8$ and 8.7 with RMS of 0.4 , and $A_0 = 165.8$ and 120.1 with RMS of 5.2 and 3.9 for PbPb and AuAu, respectively (all units in fm^2). The code can be found at <http://tglaubermc.hepforge.org/svn/branches/tools/runArea.C>.

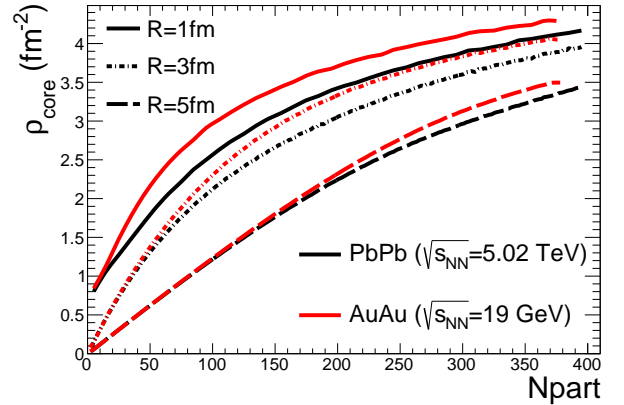


FIG. 20: Participant transverse area density in an area given by radius $R = 1, 3$ and 5 fm for AuAu collisions at $\sqrt{s_{NN}} = 19$ GeV and PbPb collisions at $\sqrt{s_{NN}} = 5.02$ TeV.

Alternatively, instead of directly using the area when estimating the energy density via the Bjorken estimate [47], one can use the participant transverse area density, ρ_{core} , which can be obtained by counting the number of participants within a core area of given radius R . Figure 20 shows ρ_{core} for various choices of R in AuAu collisions at $\sqrt{s_{NN}} = 19$ GeV and PbPb collisions at $\sqrt{s_{NN}} = 5.02$ TeV. The code can be found at <http://tglaubermc.hepforge.org/svn/branches/tools/runCore.C>